Manning, C. E., Wilke, M., Schmidt, C., Cauzid, J. (2008): Rutile solubility in albite-H2O and Na2Si3O7-H2O at high temperatures and pressures by in-situ synchrotron radiation micro-XRF. - Earth and Planetary Science Letters, 272, 3-4, 730-737

DOI: 10.1016/j.epsl.2008.06.004.

Rutile solubility in albite-H_2O and $Na_2Si_3O_7$-H_2O at high temperatures and pressures by in-situ synchrotron radiation micro-XRF

Craig E. Manning[1*], Max Wilke[2], Christian Schmidt[2] and Jean Cauzid[3]

[1]Deptartment of Earth and Space Sciences, University of California, Los Angeles CA 90095-1567, USA

[2]GeoForschungsZentrum Potsdam, Telegrafenberg, D-14473 Potsdam, Germany

[3]Département des Sciences de la Terre, Nancy-Université, G2R, 54506 Vandœuvre-lès-Nancy, France

submitted to Earth and Planetary Science Letters: Oct. 18, 2007

revision submitted June 4, 2008

*Corresponding author: email: manning@ess.ucla.edu; Tel: 1-310-206-3290; Fax: 1-310-825-2779

Abstract

Rutile is an important mineral host for high-field strength elements, so its solubility in geologic fluids at high pressure and temperature plays an important role in the crustal and mantle processes that control the terrestrial cycling of these elements. However, experimental measurements of rutile solubility are in conflict by a factor of more than 100 at most studied conditions. We performed new measurements of rutile solubility in H_2O-albite and H_2O-$Na_2Si_3O_7$ (NS3) fluids by in-situ synchrotron-radiation X-ray fluorescence spectroscopy using modified Bassett-type hydrothermal diamond-anvil cells. Minimum detection limits were 1.9 and 2.3 ppm Ti by weight for the two cells. Three albite-H_2O experiments at starting bulk compositions of 2.7, 6.7 and 10.3 wt% albite involved spectral acquisition at rutile saturation in the presence of albite crystals, melt, or a single homogeneous fluid phase; after accounting for the additional phases, corrected fluid compositions were 0.6 to 7.5 wt% dissolved silicate over the run conditions. At ≤2.7 wt% albite, rutile dissolution rate was slow and steady state was not achieved at 600–800 °C; however, at higher dissolved albite contents, constant solubility with time was observed. Rutile solubilities in the presence of a single fluid phase at 700 °C, 0.79 GPa, 5.4 wt% albite, and at 800 °C, 1.10 GPa, 6.7 wt% albite, were 37±2 and 156±6 ppm, respectively. These data agree with results acquired using hydrothermal piston-cylinder methods with long run times and suppression of new crystal growth, but not with data derived from visual observation in hydrothermal diamond-anvil cells. This discrepancy is likely due to lack of equilibrium in the latter approach. Two experiments in 10 and 30 wt% NS3 at 660–800 °C, 0.5±0.1 GPa, show extreme concentration-dependent rutile solubility enhancement to ~4500 ppm. The data indicate a strong positive correlation between rutile solubility and Na/Al. Because (Na+K)/Al is likely to be greater than unity in aqueous fluids at high pressure and temperature

45 due to incongruent dissolution of albite and micas, the increase in rutile solubility along the
46 albite-NS3 join points to the possibility of significant Ti transport by silicate-bearing aqueous
47 fluids in the lower crust and upper mantle.
48
49 **1. Introduction**
50 The high-field-strength elements (HFSE) are important tracers of processes affecting
51 magma source regions. For example, subduction-zone magmas commonly display a distinctive
52 depletion in HFSE relative to mid-ocean ridge basalt (e.g., Gill, 1981), which is widely assumed
53 to arise, at least in part, from relatively low solubility of such elements in H_2O at subduction-
54 zone conditions. Models of HFSE geochemistry at these conditions are based chiefly on
55 measurements of the solubility and partitioning behavior of rutile in geologic fluids (e.g., Ayers
56 and Watson, 1993; Brenan et al., 1994; Stalder, 1998; Foley et al., 2000), because this mineral is
57 a major host for HFSE. However, there is strong disagreement about rutile solubility in geologic
58 fluids, and the compositions of model mantle-wedge fluids that have been explored are limited.
59 Four studies have been conducted on the solubility of rutile in H_2O at high pressure (P)
60 and temperature (T): Ayers and Watson (1993), Audétat and Keppler (2005), Tropper and
61 Manning (2005) and Antignano and Manning (2008). The results give rutile solubility in H_2O
62 that are different by more than 100 times at a given P and T. For example, at 1000 °C, 2 GPa, the
63 results of Ayers and Watson yield Ti concentration in rutile saturated H_2O is 2273 ppm, whereas
64 values of 146, 109, and 14 ppm are measured or predicted respectively by Tropper and Manning
65 (2005), Antignano and Manning (2008) and Audétat and Keppler (2005). The differences are
66 much greater than the reported uncertainties in the respective studies, give changes with pressure
67 of opposite sign, and persist when components such as $NaAlSi_3O_8$ (albite) are added. Though

68 such large discrepancies caution that our understanding of the behavior of Ti – and by extension
69 other HFSE – remains poor, it might be concluded that despite large uncertainty, the generally
70 low solubilities at the conditions of interest imply that Ti is largely conserved during subduction-
71 zone metasomatic processes. However, observations of rutile in hydrothermal veins formed in
72 subduction-zone rocks (e.g., Gao and Klemd, 2001; Rubatto and Hermann, 2003; Gao et al., in
73 2007; John et al., 2008) demonstrate that geologic fluids can mobilize significant Ti (cf., Jiang et
74 al., 2005). Thus, independent of the disagreement, it is probable that previous experimental work
75 has not adequately probed the compositional space accessible to high-*P* fluids.
76 In an attempt to resolve conflicts among previous experimental studies and expand fluid
77 compositions in which rutile solubility has been measured, we conducted synchrotron-radiation
78 X-ray fluorescence (XRF) measurements on rutile-saturated albite-H_2O and $Na_2Si_3O_7$-H_2O fluids
79 in hydrothermal diamond-anvil cells. The measurements represent the first direct in-situ
80 determinations of Ti concentration in high *P*-*T* fluids, and provide a basis for evaluating the
81 controls on rutile solubility in fluids of the deep crust and upper mantle.
82
83 **2. Methods**
84 **2.1. Experimental setup**
85 The experiments employed two Bassett-type hydrothermal diamond-anvil cells (HDAC).
86 The cells were modified from the original design of Bassett et al. (1993) to optimize acquisition
87 of synchrotron-radiation XRF and X-ray absorption spectra of fluids (Schmidt & Rickers, 2003;
88 Wilke et al., 2006). Each cell had a 60-μm-deep recess (Fig. 1) in the culet face of one of the
89 anvils. In cell HDAC-A (Wilke et al., 2006), the recess was mechanically drilled and had a
90 maximum diameter of 300 μm (a conical recess ~1.5 mm deep was also drilled in the table face

91 of the same diamond). In cell HDAC-B (Schmidt & Rickers, 2003), the recess was created by
92 focused-ion-beam milling (Wirth, 2004) and had a diameter of 200 μm. The recesses permit
93 collection of the fluorescence signal at 90° to the incident beam in its polarization plane, such
94 that contributions to the signal from elastic and inelastic scattering by the sampled fluid and cell
95 components (mainly diamond) are minimized, and the fluorescence X-rays that reach the
96 detector are generated almost exclusively in the recess volume. Thus, unwanted contributions to
97 the XRF signal from phases in other portions of the sample chamber can be avoided. The path
98 length of the fluorescence X-rays through the diamonds was about 400 ± 50 μm.
99 The sample chamber of the HDACs consisted of the recess at the culet face and a
100 cylindrical hole in the Re gasket separating the two diamond anvils. The gaskets had an initial
101 thickness of 125 μm and a hole diameter of 330–510 μm. At the start of each experiment, a
102 gasket was mounted on the lower anvil. A rutile crystal, silicate glass chip and water were then
103 loaded into the gasket hole. The rutile crystal was placed on the culet face of the anvil lacking a
104 recess, at the edge of the gasket wall. This ensured that fluorescence X-rays generated by
105 excitation of Ti in rutile did not reach the detector. The silicate glass ($Na_2Si_3O_7$, NS3, or
106 $NaAlSi_3O_8$, albite) was added as a triangular chip of known thickness, which permitted accurate
107 calculation of glass volume from the chip dimensions. The mass of the glass was calculated from
108 its volume using a density of 2.4 g/cm^3 (Mazurin et al., 1983, 1987). The mass of the fluid was
109 obtained from the volume of the sample chamber (the volume of the gasket hole plus that of the
110 recess, as determined by optical micrometry), less the volume of the glass piece. Before the
111 sample chamber was sealed by slight compression of the gasket between the anvils, a small
112 amount of water was allowed to leak out until the volume ratio of the produced air bubble and
113 the remaining liquid indicated that water density upon homogenization would be ~0.6–0.7 g/cm^3.

114 Care was taken to compress the gasket just enough to seal the sample chamber. This minimized
115 the reduction of chamber volume due to gasket flow during heating. Estimated uncertainty in
116 fluid composition from all sources is ±1 wt %.
117
118 **2.2. Experimental approach**
119 The cells were heated externally by NiCr coils around the tungsten carbide seats that
120 support the anvils. Temperature was measured using K-type thermocouples attached to the
121 diamonds and controlled to within ±0.5 °C of the set value using a Eurotherm 2704 controller.
122 The actual temperature in the sample chamber was calibrated based on measurements of the
123 melting point of halite at atmospheric pressure. During heating, oxidation of metallic parts was
124 prevented by flushing the cell with 96% He – 4% H_2 gas. Utilization of this gas mixture also
125 reduced absorption of Ti Kα fluorescence X-rays along the path towards the detector.
126 Three to six heating cycles were conducted for each experiment on a particular bulk
127 composition. A typical cycle consisted of heating the cell mounted in a position for optical
128 observation and recording temperatures of phase transitions. After the desired temperature was
129 reached, the cell was rotated around the vertical axis into the position for XRF spectral
130 acquisition and aligned with the beam and the fluorescence detector. After alignment, the Ti Kα
131 signal was scanned from the position of the rutile grain towards the center of the recess to verify
132 that the recorded Ti Kα signal was solely from the fluid phase. Typically, two to three
133 consecutive XRF spectra were then recorded at a given temperature. The total time during which
134 the cell was held at each temperature was usually 40–50 min. After spectral acquisition, the cell
135 was cooled and the liquid-vapor homogenization temperature of the aqueous phase was
136 measured. This procedure was then repeated by heating the cell to a higher temperature; the

maximum temperature was 800 °C. In several cases, early cycles involved heating to low temperature and cooling, without collection of XRF spectra, chiefly to evaluate gasket behavior and/or integrity. In two cases (Table 1), the cell was not cooled between heating steps because constant homogenization temperature over consecutive cycles had established isochoric behavior.

The pressure at the experimental temperature was calculated from the equation of state of H_2O of Wagner and Pruss (2002) using the density of the aqueous fluid, as determined from its liquid-vapor homogenization temperature measured after spectral acquisition. The volumetric effect of dissolved solids in the system Na_2O-Al_2O_3-SiO_2 is assumed to be negligible. Mysen and Wheeler (2000) found that, at 1000 °C, 0.8–1.0 GPa, the density of silicate-saturated H_2O (1–6 wt% silicate) is 2–10% greater than that of pure H_2O. Their data indicate that this difference will diminish with decreasing temperature at these pressures. Accordingly, our assumption is probably reasonable for experiments with ≤10 wt% dissolved silicate; however, calculated pressure in experiment NS3-1, with 30.6 wt% dissolved silicate, is more uncertain.

2.3. XRF spectroscopy

The experiments were performed at the European Synchrotron Radiation Facility, Grenoble, France, at the micro-focus beamline ID 22. The synchrotron beam was focused to a size of 1.6 x 5 μm^2 using Kirkpatrick-Baez mirrors. The excitation energy was set to 10 keV using a Si (111) double-crystal monochromator. This energy was chosen to avoid excitation of Re L fluorescence from the gasket. The XRF spectra were recorded using a 13-element Si(Li) solid-state detector. However, only 4 elements recorded the signal due to the small aperture of the cell. The data analysis showed that the signal from the central detector element, which gave

160 the best signal-to-background ratio, was sufficient to determine the Ti concentrations because
161 adding the signal from the three other elements did not improve the signal-to-background ratio.
162 Spectral acquisition involved initial counting for 100 s, and then one or more counting periods of
163 1000 s. Net intensities of the fluorescence peaks were determined by fitting the spectra using
164 PyMCA (Solé 2006). Peak intensities were corrected for absorption in the fluid using the fluid
165 composition (silicate component and water) and density. These corrected intensities were
166 normalized to the intensity of the incoming beam. Intensities were calibrated by measurements of
167 a standard solution (1005 mg Ti/L solution; matrix: H_2O + 5 vol% HNO_3) that were loaded into
168 the sample chamber of the cell. The actual Ti concentration of the solution after loading was
169 corrected for minor evaporative loss of matrix solution by measurement of the ice melting
170 temperature in the presence of vapor (Schmidt et al. 2006, Schmidt et al. 2007). The
171 uncertainties in the actual Ti concentration of the standard solutions were 3% (HDAC-A) and 5%
172 (HDAC-B).
173 The sensitivity of the experimental setup was evaluated using spectra collected from both
174 cells when empty and when containing the standard solution (Fig. 2). All peaks other than Ti are
175 due to excitation by scattered radiation from parts of the cell or other materials in proximity to
176 the X-ray beam. The empty-cell spectrum indicates that this scattered background does not
177 contribute to the Ti signal. Estimation of absolute sensitivity (i.e., signal per mass unit) requires
178 knowledge of the excitation volume and the excited mass. We estimated the effective excitation
179 volume to be ~4.5×10^{-10} cm^3, based on the depth of the recess and the focal size of the beam.
180 Absolute sensitivities normalized to the photon flux were 1.82×10^{-11} and 2.28×10^{-11}
181 cts/s/pg/photon for HDAC A and HDAC B, respectively; relative sensitivities normalized to the
182 photon flux were 8.17×10^{-15} (A) and 1.03×10^{-14} cts/s/ppm/photon (B). The absolute and relative

183 values indicate a 25% difference between the two cells. The fact that the size of excited volume
184 need not be known for the relative sensitivity shows that the excitation volumes of the two cells
185 must be similar, regardless of the exact size of this volume. Otherwise absolute and relative
186 sensitivities would differ under the given assumptions.

187 The minimum detection limit (*mdl*) was calculated from $mdl = 3c\sqrt{B} / I$ (e.g. Haller &
188 Knöchel 1996), where *c* is the concentration, *B* the background intensity and *I* the peak intensity.
189 The *mdl* values determined from standard-solution spectra were 1.9 ppm for HDAC-A and 2.3
190 ppm for HDAC-B. The standard deviation provided in Table 1 is propagated from the
191 uncertainty in the Ti intensity from the fits of the spectra and the uncertainty of the
192 concentrations in the standard solutions.
193

194 **2.4. Fluid composition**

195 The NS3 glass dissolved completely in H_2O to produce one fluid at all experimental
196 conditions, but albite glass did so only at the lowest concentrations or the highest *P* and *T*. Where
197 an additional phase was present (albite crystals or melt), fluid composition was calculated from
198 polynomial fits to the isothermal variation in albite solubility with *P* (Anderson and Burnham,
199 1983). The investigated conditions were generally within the range of the data of Anderson and
200 Burnham (1983) or required only minor extrapolation; fluid compositions so determined were
201 assumed to be accurate to ±1 wt%. However, at the highest *P*, *T* and albite concentration
202 investigated (Table 1), melt was present instead of albite crystals. In this case, melt solubility
203 was assumed to be the same as albite solubility, as predicted by extrapolation of the Anderson
204 and Burnham (1983) data to 800 °C, but assigned a larger uncertainty of ±2 wt%. All Ti
205 concentrations are reported as mg per kg solution (ppm).

3. Results and discussion

We determined Ti concentrations in the presence of rutile at high *P* and *T* for three albite-H_2O bulk compositions and two NS3-H_2O bulk compositions. Results are given in Table 1 and Fig. 3.

3.1. Phases present

Depending on bulk composition, phases present with rutile at the *P-T* of spectral acquisition were fluid+crystals, fluid+melt (Fig. 1a) or a single fluid phase (Fig. 1b). In the albite-H_2O experiments, the crystals were assumed to be albite, based on the observed transitions from crystals to melt (Albite-1) and to a single fluid (Albite-2) at 700–800 °C at 0.8–1.1 GPa (Table 1), which are similar to conditions determined independently (e.g., Stalder et al. 2000). Previous work has shown that albite dissolves incongruently at high *P* and *T* (Currie, 1968; Anderson and Burnham, 1983; Stalder et al., 2000; Shmulovich et al., 2001); however, no other residual minerals were observed. We infer that experiment durations were shorter than required for nucleation of any residual phases.

The NS3-H_2O experiments were supersaturated with respect to quartz at some conditions (Table 1). In NS3-2, quartz formed upon heating during cycle 5. These crystals dissolved at 757 °C. After the NS3-1 cycle 3, crystals formed at about 500 °C upon reheating and did not completely dissolve during further heating. These crystals were identified as quartz by Raman spectroscopy after the experiments. The formation of quartz in the cell after significant time at elevated *T* is consistent with the strong nucleation barrier for this phase. Experiments were terminated whenever quartz was observed in the cell.

228 **3.2. Reproducibility and equilibrium**

229 We evaluated reproducibility in experiment Albite-2 (Table 1) by collecting spectra at
230 700 °C, cooling, then reheating to 700 °C and collecting additional spectra. The two analysis
231 cycles gave the same concentration within 1σ (Table 1, Fig. 3b).

232 Variations in counting time allowed us to assess the approach to equilibrium in the
233 experiments. Based on time-resolved XRF analyses of fluid during monazite and zircon
234 dissolution experiments in acidic solutions (Schmidt et al. 2006, Schmidt et al. 2007) and
235 previous study of rutile solubility in HDACs (Audétat & Keppler 2005), we expected that the
236 equilibration time would be of the order of several minutes. However, the data suggest that in the
237 albite-H_2O experiments, there were concentration-dependent variations in equilibration time
238 (Fig. 3). This was established by estimating the elapsed time after an experiment had been
239 brought to a particular temperature from the log files, which was possible to within ±5 min. At
240 the lowest *T*, *P* and dissolved silicate (600 °C, 0.31 GPa, 0.6 wt% albite), measured Ti
241 concentration after 39 min is higher than that after 22 min by ~2σ. An increase in Ti
242 concentration with time was observed during all cycles and times in experiment Albite-3 (2.7
243 wt% albite; Fig. 3a). At 5.4 wt% albite (Albite-2), Ti concentration after 6 min at 700 °C is lower
244 than at longer elapsed times, but by less than 1σ. Finally, at 6.7 and 7.5 wt% albite, Ti
245 concentration was constant at ≥6 min (Fig. 3b). Both NS3-H_2O experiments yielded constant
246 solubility with time (Fig. 3c). It is possible that the behavior of experiment Albite-3 was caused
247 by change in the excitation volume in the recess of HDAC-A due to a slow change in position
248 when the cell holder was not thermally equilibrated; however, this is unlikely because the
249 behavior was not observed in all experiments. Instead, it appears that the time required for
250 equilibration in albite solutions is at least several minutes in all cases, and significantly longer

(more than several tens of minutes) at low dissolved albite content. Fig. 3 shows weighted mean Ti concentrations for those experiments interpreted to have reached equilibrium.

3.3. Rutile solubility in albite-bearing H_2O

The equilibrium data indicate that Ti solubility at rutile saturation is 37±2 ppm at 700 °C, 0.79 GPa and 5.4 wt% dissolved albite. Higher solubility of 155±6 ppm was obtained at 800 °C, 1.11 GPa and 6.7 wt% albite. A general increase in solubility with *T*, *P* and/or dissolved albite concentration is consistent with previous findings (Audétat and Keppler, 2005; Antignano and Manning, 2008); however, prior experimental studies yield quite different absolute rutile solubilities in H_2O and albite-H_2O at high *P* and *T*. Our results provide additional, independent constraints on this system.

The previous experimental studies on rutile solubility in aqueous solutions at high *P* and *T* have employed contrasting approaches. Using hydrothermal piston-cylinder weight-loss techniques (Manning, 1994; Manning and Boettcher, 1994), Tropper and Manning (2005) and Antignano and Manning (2008) measured rutile solubility in H_2O at 700–1150 °C, 0.7–2.0 GPa and obtained much lower values than Ayers and Watson (1993), who used similar methods. Tropper and Manning (2005) attributed the differences to misinterpretation of recrystallized rutile as quench in the experiments of Ayers and Watson (1993). Audétat and Keppler (2005) used visual observation of rutile growth and dissolution in the HDAC and found rutile solubilities in H_2O lower than Tropper and Manning (2005) and Antignano and Manning (2008) by nearly 10 times. A similar discrepancy exists for albite-H_2O solutions. Antignano and Manning (2008) determined rutile solubility in albite-H_2O at 0.7–2.0 GPa, 700–900 °C, and also derived solubilities that were higher than those of Audétat and Keppler (2005) at similar fluid

compositions by up to 100 times. Although the stoichiometry of dissolved silicate differed (Antignano and Manning (2008) noted incongruent albite dissolution, but Audétat and Keppler (2005) did not), the disparity was no more than 15% and unlikely to explain the disagreement. The large discrepancies have led to the suggestion that hydrothermal piston-cylinder experiments using weight-loss techniques are unreliable because of difficulty in accounting for new growth of the phase of interest (Audétat and Keppler, 2005).

We collected spectra at two separate conditions where rutile coexisted with only an albite-bearing aqueous phase. These measurements are compared with those of Audétat and Keppler (2005) and Antignano and Manning (2008) at 700 and 800 °C in Fig. 4. Both previous studies indicate an increase in rutile solubility with increasing albite concentration at high *P* and *T*. At 700 °C, our measured rutile solubility at 0.79 GPa is within error of the 1 GPa data of Antignano and Manning (2008) (Fig. 4a). Antignano and Manning (2008) found that, at fixed *T* and albite content, rutile solubility increases slightly with pressure; however, at 700 °C, ≤1 GPa, the effect is predicted to be smaller than the uncertainty in the 1 GPa data.

Figure 4b compares results on rutile solubility in albite-H_2O at 800 °C and a range of *P*. The data of Antignano and Manning (2008) at 1.0 and 1.5 GPa suggest increasing solubility with *P*. Our measurement at 1.1 GPa lies between the 1.0 and 1.5 GPa isopleths of Antignano and Manning (2008), although closer to the 1.5 GPa datum. However, we obtained a Ti concentration that is significantly higher than that inferred by Audétat and Keppler (2005) at similar *P* (Fig. 4b). The explanation for this difference is most likely the surprisingly slow reaction rates of rutile dissolution, as indicated by the present study. Audétat and Keppler determined solubility by visually monitoring the appearance and disappearance of rutile crystals in an HDAC using heating rates of tens of degrees per minute. If reaction rates are slow, this method will lead to

297 overstepping of the temperature at which complete dissolution would occur had the cell been
298 held at a lower *T* for longer time. The result would be low apparent solubility, as observed when
299 comparing the results of Audétat and Keppler (2005) to studies involving equilibration times of
300 tens of minutes (this study) to hours (Antignano and Manning, 2008).
301
302 **3.4. Rutile solubility in albite-bearing H_2O saturated with hydrous melt**
303 Our third measurement of rutile solubility in albite-H_2O in which equilibrium can be
304 inferred was at 800 °C, 0.71 GPa, in the presence of hydrous albite melt and fluid with ~7.5 wt%
305 albite. Rutile solubility was 185 ± 9 ppm Ti. In this case, our Ti concentration is significantly
306 higher than that which would be predicted from Audétat and Keppler (2005) or Antignano and
307 Manning (2008). It is also higher than would be predicted from experiment Albite-2 if rutile
308 solubility increases with *P* as proposed by Antignano and Manning (2008). In light of the
309 generally good agreement between our results and those of Antignano and Manning (2008) in the
310 presence of a single fluid phase, we infer that the presence of melt led to anomalously high Ti
311 concentrations. Hydrous albite melt partitions Ti strongly relative to the fluid phase (Hayden and
312 Watson, 2007; Antignano and Manning, 2008). We suggest that excess Ti was measured due to
313 fluorescence of Ti in melt blebs in the sample chamber (Fig. 1a).
314
315 **3.5. Rutile solubility in NS3-H_2O**
316 Figure 5 shows the variation in rutile solubility with NS3 content in NS3-H_2O fluid at
317 660–800 °C, 0.5±0.1 GPa, to >30 wt% NS3. The fluid is everywhere in the one-phase field,
318 though the system was metastable with respect to quartz at some conditions (Table 1). Assuming
319 that there is negligible dependence on *P* over this small interval, the results indicate that Ti

concentration rises with T at constant fluid composition. The T dependence of solubility in pure H_2O is strong (Antignano and Manning, 2008); however, this dependence appears to diminish with increasing NS3, such that at 30.6 wt% NS3, Ti concentrations are nearly identical within the uncertainties in the investigated T range. These features are reproduced by the following fit equation:

$$\log c_{\mathrm{Ti}} = \log c_{\mathrm{Ti}}^{\circ} + \left(1.71 - 1.07 \times 10^{-3} T\right) c_{\mathrm{NS3}}^{0.44} \quad (1)$$

where T is in K, c_{NS3} is NS3 concentration in wt%, c_{Ti} is Ti concentration in ppm, and c_{Ti}° is Ti concentration in pure H_2O in equilibrium with rutile (also in ppm), as calculated from:

$$\log c_{\mathrm{Ti}}^{\circ} = 6.173 - 5425 / T + 1.784 \times 10^{-2} P / T \quad (2)$$

(Antignano and Manning, 2008), where T is again in K and P is in GPa. The increase in rutile solubility with NS3 content is strongly nonlinear, such that very high solubilities – up to 0.4 wt% Ti – are suggested in these peralkaline solutions.

4. Implications for high *P-T* fluids

The present results can be used to place preliminary constraints on the nature of Ti dissolution mechanisms at high P and T. As shown in Fig. 4, dissolved albite enhances rutile solubility at a given P and T (Audétat and Keppler, 2005; Antignano and Manning, 2008). Rutile solubility is also enhanced by NS3 (Fig. 5). The degree of enhancement can be compared at 700 °C, 0.8 GPa, where dissolved Ti concentration in pure H_2O is 18 ppm (Antignano and Manning,

343 2008). Addition of 5.4 wt% albite increases solubility to 37±2 ppm; however, a similar
344 concentration of NS3 would have a Ti concentration of 250 ppm (Eq. 1). Thus, on an equivalent-
345 weight basis, NS3 yields nearly ten times greater enhancement of rutile solubility.
346 The observation that rutile solubility is higher in Al-free Na-silicate-bearing fluid than in
347 albite-bearing fluid is similar to results on rutile solubility in silicate melts. Dickenson and Hess
348 (1985) found that rutile solubility in K_2O-Al_2O_3-SiO_2 melts increased isothermally and
349 isobarically with increasing K_2O/Al_2O_3. For more complex natural magmas, Ryerson and
350 Watson (1987) used the compositional parameter $FM = [Na + K + 2(Ca + Fe + Mg)]Al^{-1}Si^{-1}$ to
351 examine the role of melt composition on rutile solubility. Their results indicate that at constant
352 concentrations of Si and divalent cations, rutile solubility increases with increasing FM, which
353 corresponds to increasing (Na+K)/Al. Similar results were obtained by Hayden and Watson
354 (2007) on hydrous melts. The increase in Ti solubility with increasing (Na+K)/Al is consistent
355 with the low melting temperatures in the Na_2O-TiO_2-SiO_2 system (Hamilton and Cleek, 1958;
356 Glasser and Marr, 1979). These observations suggest formation of alkali-titanate complexes in
357 the melt (Dickenson and Hess, 1985).
358 The results of the present study suggest that, as in silicate melts, Na-Ti complexing may
359 be important in controlling rutile solubility in high *P*-*T* fluids. Na-Al silicates dissolved in H_2O at
360 these conditions form a wide range of solute complexes, but a significant fraction of these
361 complexes are polymerized Al-Si species with one or more bridging oxygens and charge-
362 balancing Na (Manning, 2004, 2007). If this is correct, then Al-free solutions are likely to be less
363 polymerized. The strong inverse correlation between aqueous Al and Ti concentrations suggests
364 that greater dissolved Ti may be accommodated by liberation of Na as Al-Si polymer
365 concentrations decrease.

366 An increase in Ti concentration with increasing Na/Al is significant because fluids in
367 equilibrium with albite have Na/Al > 1 due to incongruent dissolution of albite (e.g., Anderson
368 and Burnham, 1983; Stalder et al., 2000). Moreover, this ratio increases with increasing *P*
369 (Anderson and Burnham, 1983; Antignano and Manning, in preparation). Thus, the expected
370 increase in rutile solubility with increasing *P* will be compounded by increasing peralkalinity of
371 the fluid phase. As a result, high dissolved Ti concentrations are to be expected in Al-poor
372 environments metasomatized by fluids derived from Na-Al-silicate-bearing lithologies, such as
373 the mantle wedge above subducting oceanic slabs. It has been hypothesized that low-silica, Ti-
374 rich adakites are melts of the mantle wedge that has been metasomatically enriched in Ti and
375 other HFSE by felsic melts derived from the subducting slab (e.g., Martin et al., 2005). The
376 results of the present study suggest that the mobility of Ti, and by analogy other HFSE, may be
377 sufficiently high in appropriate fluid compositions that slab melting need not be invoked to
378 explain HFSE-enriched subduction-zone magmas.
379
380 **5. Conclusions**
381 (1) The measurements of standard solutions and of albite-H_2O and NS3-H_2O fluids at
382 rutile saturation at high *P* and *T* indicate excellent sensitivity and reproducibility for the analysis
383 of Ti by synchrotron-radiation XRF in hydrothermal diamond anvil cells. Precisions of ~5-10%
384 relative (1σ) at low Ti concentration are a significant improvement over other methods where
385 precision may be no better than 50% relative (Audétat and Keppler, 2005; Tropper and Manning,
386 2005; Antignano and Manning, 2008). In addition, our methods permit the approach to
387 equilibrium to be monitored directly by collection of multiple spectra over time. The minimum
388 detection limit of <3 ppm suggests that the techniques described in this paper offer excellent

prospects for evaluation of rutile solubility and dissolution kinetics at relatively low *P* and *T*, where Ti concentrations are expected to be quite low.

(2) The solubility of rutile in albite-H_2O fluids increases with *P*, *T* and dissolved albite content. Our results agree well with those of Antignano and Manning (2008), but not with those of Audétat and Keppler (2005). We infer that the rate of the rutile dissolution reaction is unexpectedly slow, which led to overstepping of the dissolution equilibrium and underestimation of rutile solubility in the latter study. Our data indicate that hydrothermal piston-cylinder and HDAC approaches to the determination of mineral solubility can be reconciled.

(3) The solubility of rutile in NS3-H_2O fluids exhibits a strong positive correlation with dissolved silicate. Peralkaline fluids can be expected to transport significant Ti in lower crustal and mantle environments.

(4) The increase in rutile solubility with increasing Na/Al points to a Ti dissolution mechanism involving Na-Ti complexing, as in silicate melts.

(5) The high Ti concentrations in fluids with Na/Al > 1 is important because it is likely that such ratios characterize fluids metasomatizing the mantle wedge. The ability of this type of fluid to transport Ti suggests an alternative mechanism for HFSE enrichment in the source of low-silica adakites.

Acknowledgments

We thank H.J. Reichmann for assistance with the measurements. The manuscript was improved by comments on an early draft by R. Newton, a journal review by J. Brenan, and editorial handling by R. Carlson. The research was funded through support from the ESRF, U.S.

National Science Foundation grants EAR-0337170 and 0711521, and the German Academic Exchange Service (DAAD).

References

Anderson, G.M., Burnham, C.W., 1983. Feldspar solubility and the transport of aluminum under metamorphic conditions. Am. J. Sci. 283-A, 283–297.

Antignano, A., Manning, C.E., 2008. Rutile solubility in H_2O and H_2O-albite at 700–1000 °C and 0.7–2.0 GPa: implicatations for the aqueous transport of high-field-strength elements at high pressure and temperature. Chem. Geol., in press.

Audétat , A., Keppler, H., 2005. Solubility of rutile in subduction zone fluids, as determined by experiments in the hydrothermal diamond anvil cell. Earth Planet. Sci. Lett. 232, 393–402.

Ayers, J.C., Watson, E.B., 1993. Rutile solubility and mobility in supercritical aqueous fluids. Contrib. Mineral. Petrol. 114, 321–330.

Bassett, W.A., Shen, A.H., Bucknum, M., Chou, I-M., 1993. A new diamond anvil cell for hydrothermal studies to 2.5 GPa and from -190 to 1200 °C. Rev. Sci. Instrum. 64, 2340–2345.

Brenan, J.M., Shaw, H.F., Phinney, D.L., and Ryerson, F.J., 1994. Rutile-aqueous fluid partitioning of Nb, Ta, Hf, Zr, U and Th: implications for high field strength element depletions in island-arc basalts. Earth Planet. Sci. Lett. 128, 327–339.

Currie, K.L., 1968. On the solubility of albite in supercritical water in the range 400 to 600 °C and 750 to 3500 bars. Am. J. Sci. 266, 321–341.

Defant, M.J., Drummond, M.S., 1990. Derivation of some modern arc magmas by melting of young subducted lithosphere. Nature 347, 662–665.

434 Dickenson Jr., J.E., Hess, P.C., 1985. Rutile solubility and titanium coordination in silicate melts.
435 Geochim. Cosmochim. Acta 49, 2289–2296.
436 Foley, S.F., Barth, M.G., Jenner, G.A, 2000. Rutile/melt partition coefficients for trace elements
437 and an assessment of the influence of rutile on the trace element characteristics of subduction
438 zone magmas. Geochim. Cosmochim. Acta 64, 933–938.
439 Gao, J., Klemd, R., 2001. Primary fluids entrapped at blueschist to eclogite transition: evidence
440 from the Tianshan meta-subduction complex in northwestern China. Contrib. Mineral. Petrol.
441 142, 1–14.
442 Gao, J., John, T., Klemd, R., Xiong, X.M., 2007. Mobilization of Ti-Nb-Ta during subduction:
443 evidence from rutile-bearing dehydration segregations and veins hosted in eclogite, Tianshan,
444 NW China. Geocim. Cosmochim. Acta 71, 4974–4996..
445 Gill, J.B., 1981. Orogenic Andesites and Plate Tectonics. Springer-Verlag, Berlin.
446 Glasser, F.P, Marr, J., 1979. Phase relations in the system Na_2O-TiO_2-SiO_2. J. Am. Ceram. Soc.
447 62, 42–47.
448 Haller, M., Knöchel, A., 1996. X-ray fluorescence analysis using synchrotron radiation
449 (SYXRF). J. Trace Microprobe Techniques. 14, 461–488.
450 Hamilton, E.H., Cleek, G.W., 1958. Properties of sodium titanium silicate glasses. J. Res. Nat.
451 Bur. Standards 61, 89–94.
452 Hayden, L.A., Watson, E.B., 2007. Rutile saturation in hydrous siliceous melts and its bearing on
453 Ti-thermometry of quartz and zircon. Earth Planet. Sci. Lett. 258, 561–568.
454 Jiang, S.Y., Wang, R.C., Xu, X.S., Zhao, K.D., 2005. Mobility of high field strength elements
455 (HFSE) in magmatic-, metamorphic-, and submarine-hydrothermal systems. Phys. Chem.
456 Earth 30, 1020–1029.

457 John, T., Klemd, R., Gao, J., and Garbe-Schönberg, C.-D., 2008. Trace-element mobilization in
458 slabs due to non steady-state fluid-rock interaction: constraints from an eclogite-facies
459 transport vein in blueschist (Tianshan, China). Lithos 103, 1-24.
460 Manning, C.E., 1994. The solubility of quartz in H_2O in the lower crust and upper mantle.
461 Geochim. Cosmochim. Acta 58, 4831–4839.
462 Manning, C.E., 2004. The chemistry of subduction-zone fluids. Earth Planet. Sci. Lett. 223, 1–
463 16.
464 Manning, C.E., 2007. Solubility of corundum + kyanite in H_2O at 700 °C and 10 kbar: Evidence
465 for Al-Si complexing at high pressure and temperature. Geofluids 7, 258–269.
466 Manning, C.E., Boettcher, S.L., 1994. Rapid-quench hydrothermal experiments at mantle
467 pressures and temperatures. Am. Mineral. 79, 1153–1158.
468 Martin, H., Smithies, R.H., Rapp, R., Moyena, J.-F., Champion, D., 2005, An overview of
469 adakite, tonalite–trondhjemite–granodiorite (TTG),and sanukitoid: relationships and some
470 implications for crustal evolution. Lithos 79, 1–24.
471 Mazurin, O.V., Streltsina, M.V., Shviko-Shvikovskaya, T.P., 1983. Handbook of Glass Data,
472 Part A. Silica Glass and Binary Silicate Glasses. Elsevier, Amsterdam.
473 Mazurin, O.V., Streltsina, M.V., Shviko-Shvikovskaya, T.P., 1987. Handbook of Glass Data,
474 Part C. Ternary Silicate Glasses. Elsevier, Amsterdam.
475 Mysen, B.O., Wheeler, K., 2000. Alkali aluminosilicate-saturated fluids in the earth's upper
476 mantle. Geochim. Cosmochim. Acta 64, 4243–4256.
477 Rubatto, D., Hermann, J., 2003. Zircon formation during fluid circulation in eclogites (Monviso,
478 Western Alps): implications for Zr and Hf budget in subduction zones. Geochim.
479 Cosmochim. Acta 67, 2173–2187.

480 Ryerson, F.J., Watson, E. B., 1987. Rutile saturation in magmas: implications for Ti-Nb-Ta
481 depletion in island-arc basalts. Earth. Planet. Sci. Letters 86, 225–239.
482 Solé, V.A., Papillon, E., Cotte, M., Walter, P., Susini, J., 2007. A multiplatform code for the
483 analysis of energy-dispersive X-ray fluorescence spectra. Spectrochim. Acta B 62, 63–68.
484 Schmidt, C., Rickers, K., 2003. In-situ determination of mineral solubilities in fluids using a
485 hydrothermal diamond-anvil cell and SR-XRF: Solubility of AgCl in water. Am. Mineral. 88,
486 288–292.
487 Schmidt, C., Rickers, K., Wirth, R., Nasdala, L., Hanchar, J.M., 2006. Low-temperature Zr
488 mobility: An in situ synchrotron-radiation XRF study of the effect of radiation damage in
489 zircon on the element release in H_2O + HCl ± SiO_2 fluids. Am. Mineral. 91, 1211–1215.
490 Schmidt, C., Rickers, K., Bilderback, D.H., Huang, R., 2007. In situ synchrotron-radiation XRF
491 study of REE phosphate dissolution in aqueous fluids to 800 °C. Lithos 95, 87–102.
492 Shmulovich, K.I., Graham, C., Yardley, B., 2001. Quartz, albite and diopside solubilities in H_2O-
493 NaCl and H_2O-CO_2 fluids at 0.5–0.9 GPa. Contrib.. Mineral. Petrol. 141, 95–108.
494 Solé, V.A., Papillon, E., Cotte, M., Walter, P., Susini, J., 2007. A multiplatform code for the
495 analysis of energy-dispersive X-ray fluorescence spectra. Spectrochim. Acta B 62, 63–68.
496 Stalder, R., Foley, S.F., Brey, G.P., Horn, I., 1998. Mineral-aqueous fluid partitioning of trace
497 elements at 900–1200 °C and 3.0–5.7 GPa: new experimental data for garnet, clinopyroxene,
498 and rutile, and implications for mantle metasomatism. Geochim. Cosmochim. Acta 62, 1781–
499 1801.
500 Stalder, R., Ulmer, P., Thompson, A.B., Günther, D., 2000. Experimental approach to constrain
501 second critical end points in fluid/silicate systems: Near-solidus fluids and melts in the
502 system albite-H_2O. Am. Mineral. 85, 68–77.

503 Tropper, P., Manning, C.E., 2005. Very low solubility of rutile in H_2O at high pressure and
504 temperature, and its implications for Ti mobility in subduction zones. Am. Mineral. 90, 502–
505 505.
506 Wagner, W., Pruss, A., 2002. The IAPWS formulation 1995 for the thermodynamic properties of
507 ordinary water substance for general and scientific use. J. Phys. Chem. Ref. Data 31, 387–
508 535.
509 Wilke, M., Schmidt, C., Farges, F., Malavergne, V., Gautron, L., Simionovici, A., Hahn, M.,
510 Petit, P.-E., 2006. Structural environment of iron in hydrous aluminosilicate glass and melt –
511 evidence from X-ray absorption spectroscopy. Chem. Geol. 229, 144–161.
512 Wirth, R., 2004. Focused Ion Beam (FIB): A novel technology for advanced application of
513 micro- and nanoanalysis in geosciences and applied mineralogy. Eur. J. Mineral. 16, 863–
514 877.

Figure captions

Fig. 1. Photomicrographs of horizontally mounted HDAC, showing sample chambers with recesses. View toward X-ray beam. Upper image shows HDAC A at high *P* and *T*, at conditions of hydrous albite melt + aqueous fluid stability. Rutile crystal is on culet face at base of cell; recess contains fluid + melt. Lower image shows HDAC B at high P-T where only a single fluid phase is stable.

Fig. 2. X-ray fluorescence spectra of empty cell (lower) and cell filled with standard solution (upper). The standard solution contained 993 ppm Ti, based on correction for evaporation after loading of standard solution with 1005 ppm Ti. Comparison of the two spectra shows negligible Ti background in the empty cell. All other peaks are due to excitation by scattered radiation of the diamond cell and other materials in the vicinity of the beam path.

Fig. 3. Ti concentration in rutile-saturated fluids as a function of elapsed time at the measurement *P-T* condition. Elapsed time is the time between attainment of experimental temperature and completion of counting; uncertainty is ±5 min (see text). Symbols keyed to experimental *P*, *T* and fluid composition listed at right; open and filled symbols for the same conditions denote different cycles (Table 1). Errors in Ti concentration are 1σ. Horizontal dashed lines show mean Ti concentrations in those experiments interpreted to have attained equilibrium, weighted by $1/\sigma^2$; values given at right with experimental conditions (see text).

Fig. 4. Ti concentrations vs. dissolved silicate concentration at 700 °C (A) and 800 °C (B); all errors 2σ. In (A), datum from the present study is compared to results of Antignano and Manning

538 (2008) at 1.0 GPa (data, filled circles; fit equation, solid lines). In (B), data from this study are
539 compared to Antignano and Manning (2008) data (1.0 GPa, filled circles, pure-H_2O datum is
540 weighted mean of 3 experiments; 1.5 GPa, open circle) and fit equations (solid lines), as well as
541 to results of Audétat and Keppler (2005; filled squares; pure H_2O datum is calculated from their
542 fit equation and uncertainty is assumed to be 30% relative, based on data in their Table 1).
543 "Dissolved silicate" in this study and Audétat and Keppler (2005) is albite; however Antignano
544 and Manning (2008) observed incongruent dissolution of albite to paragonite/corundum + fluid,
545 so their fluid compositions differ slightly from the other studies. The error bars on their data
546 show the range in dissolved silicate concentration from a maximum for albite stoichiometry (i.e.,
547 negligible mass of residual phases) to a minimum derived from fits to the variation in
548 concentration at 600 °C with increasing P (Antignano and Manning, 2008).
549
550 **Fig. 5.** Ti concentration vs. dissolved $Na_2Si_3O_7$ concentration at 660 to 800 °C at 0.5 ±0.1 GPa.
551 2σ uncertainties are smaller than symbol sizes. Pure H_2O values calculated from Equation (2) of
552 Antignano and Manning (2008). Solid lines calculated from Equation (1).

Table
Click here to download Table: table 1.doc

Table 1. Experimental results.

Cycle	Temperature (°C)	Pressure (GPa)	Acquisition time (s)	Elapsed time (min)	Dissolved silicate (wt%)	Ti (ppm)	Phases	Remarks
Albite-3, HDAC-A, bulk composition: 2.7 wt% Albite								
2	700	1.23	1000	29	2.7	64(5)	F	
2	700	1.23	1000	46	2.7	77(5)	F	
3	752	1.30	1000	19	2.7	107(7)	F	
3	752	1.30	1000	37	2.7	127(7)	F	
5	800	1.19	100	3	2.7	152(15)	F	
5	800	1.19	1000	21	2.7	156(9)	F	
5	800	1.19	1000	39	2.7	183(10)	F	
Albite-2, HDAC-A, bulk composition: 6.7 wt% Albite								
2	700	0.79	100	6	5.4*	31(6)	XF	
2	700	0.79	1000	24	5.4*	37(3)	XF	
2	700	0.79	1000	42	5.4*	37(3)	XF	
3	700	0.79	100	24	5.4*	32(6)	XF	Cell reheated to 700°C
3	700	0.79	1000	42	5.4*	39(3)	XF	
3	800	1.11	100	15	6.7	153(17)	F	Heated from 700°C
3	800	1.11	1000	34	6.7	145(9)	F	
3	800	1.11	1000	52	6.7	168(9)	F	
Albite-1, HDAC-A, bulk composition: 10.3 wt% Albite								
4	600	0.31	1000	22	0.6*	4(1)	XF	Heated from 500°C
4	600	0.31	1000	39	0.6*	6(1)	XF	
5	700	0.44	1000	20	1.6*	19(2)	XF	
6	800	0.71	100	4	7.5*	185(17)	MF	X→M at 762°C
6	800	0.71	1000	23	7.5*	185(10)	MF	
NS3-2, HDAC-B, bulk composition: 9.3 wt% NS3								
3	660	0.34	1000	27	9.3	214(15)	F	Qz supersaturated
4	730	0.44	100	11	9.3	251(25)	F	Qz supersaturated
4	730	0.44	1000	29	9.3	286(20)	F	Qz supersaturated
5	800	0.59	100	2	9.3	406(37)	F	
5	800	0.59	1000	20	9.3	410(28)	F	
NS3-1, HDAC-B, bulk composition: 30.6 wt% NS3								
1	660	0.36	1000	40	30.6	4490(272)	F	Qz supersaturated
2	730	0.49	100	22	30.6	4019(277)	F	Qz supersaturated
2	730	0.49	1000	40	30.6	3986(242)	F	Qz supersaturated
3	800	0.62	100	13	30.6	4266(298)	F	Qz supersaturated
3	800	0.62	1000	31	30.6	4410(268)	F	Qz supersaturated

Explanation: Bulk composition determined from mass H_2O and silicate glass at start of each experiment; actual fluid composition at high *P-T* changed with phases present. Elapsed time is the time at end of spectral acquisition less the ttime at which heating to the experimental temperature was completed. Abbreviations: X: Subsolidus region, crystals inferred to be albite present; F: aqueous fluid; M: silicate melt. Asterisk indicates dissolved silicate calculated by polynomial fits, extrapolated where necessary, to experimentally determined albite solubility in H_2O (Anderson and Burnham, 1983); estimated error is ±1 wt%. Dissolved silicate in melt-saturated H_2O approximated using the same equations, but estimated error is larger (±2 wt%). Parenthetical numbers denote 1σ errors in last significant digits.

Figure

Click here to download Figure: fig 1.pdf

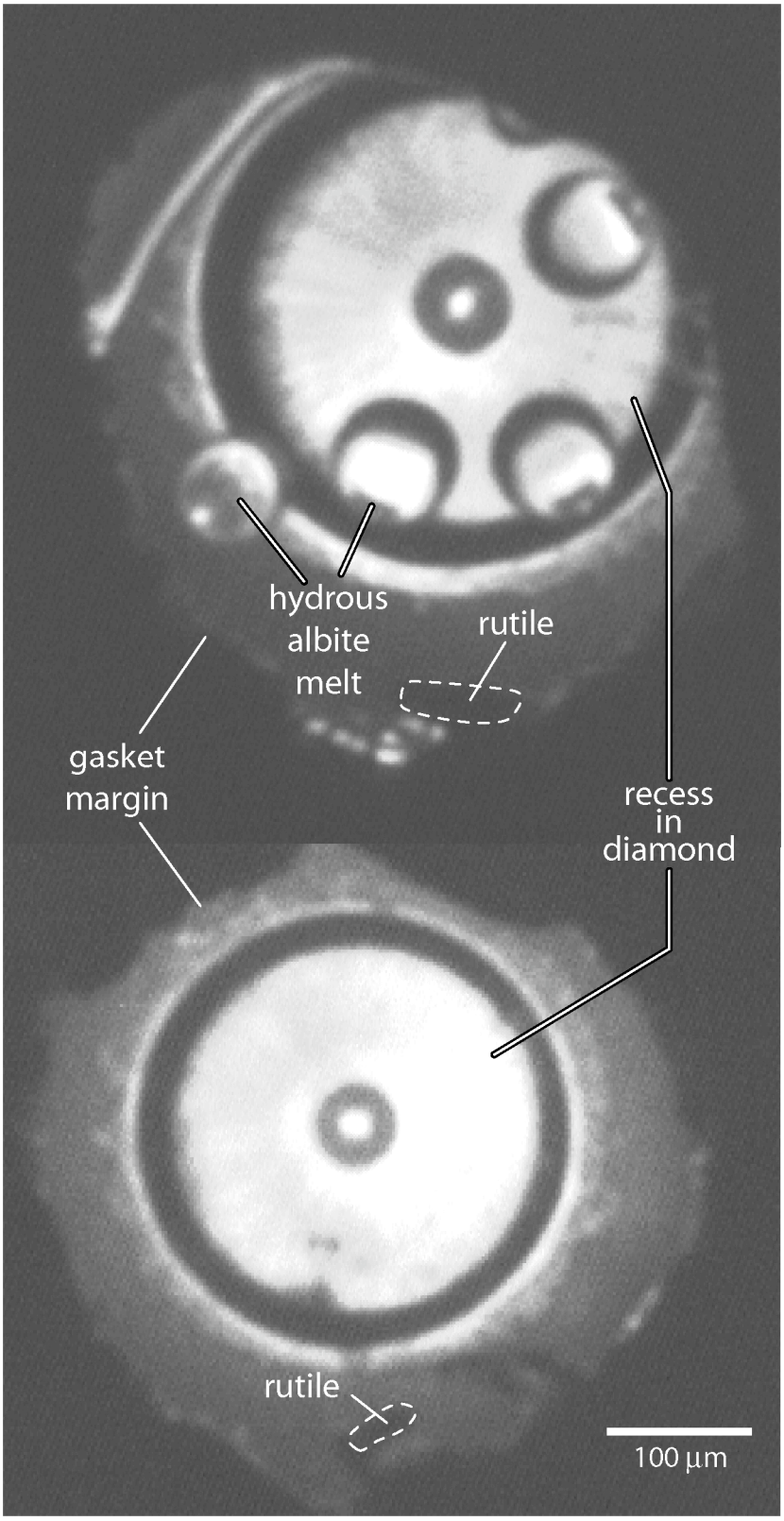

Manning et al., Fig. 1

Figure
Click here to download Figure: fig 2 2.pdf

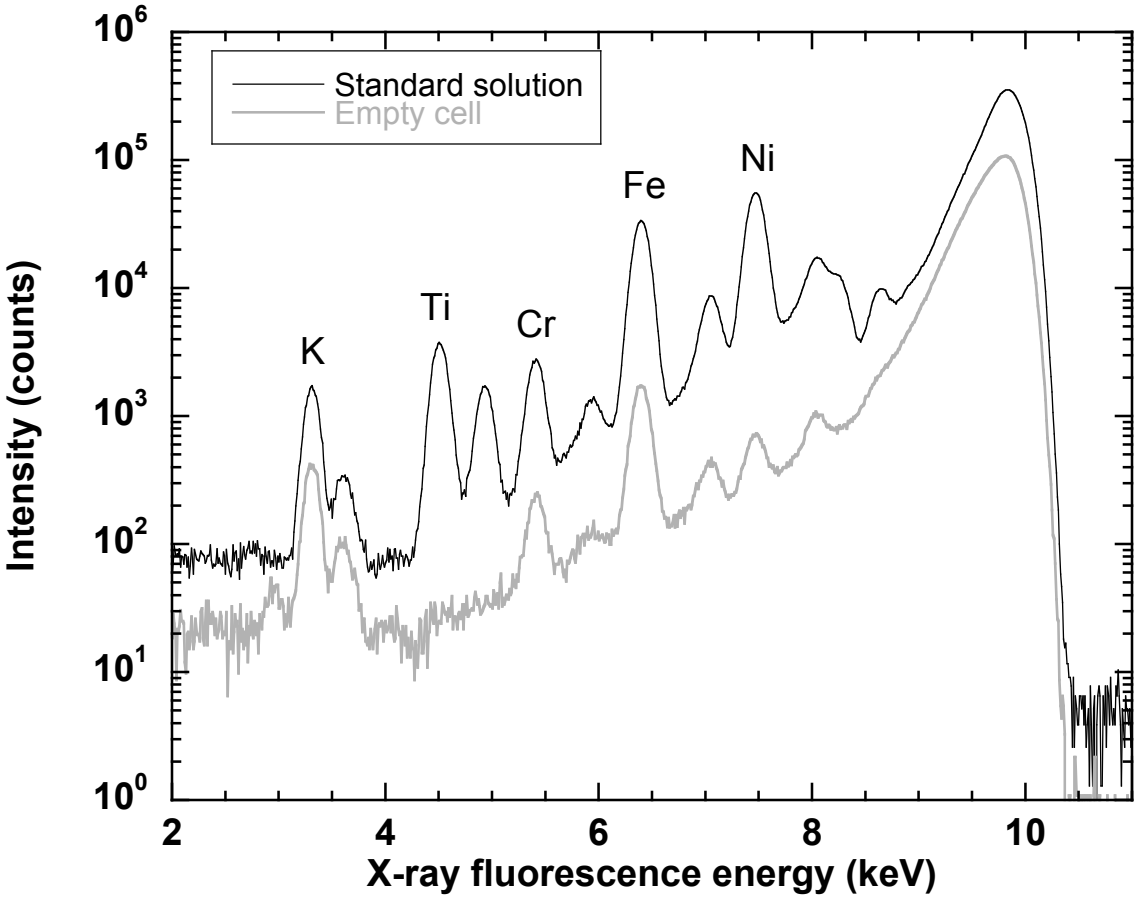

Manning et al., Fig. 2

Figure
Click here to download Figure: fig 3 2.pdf

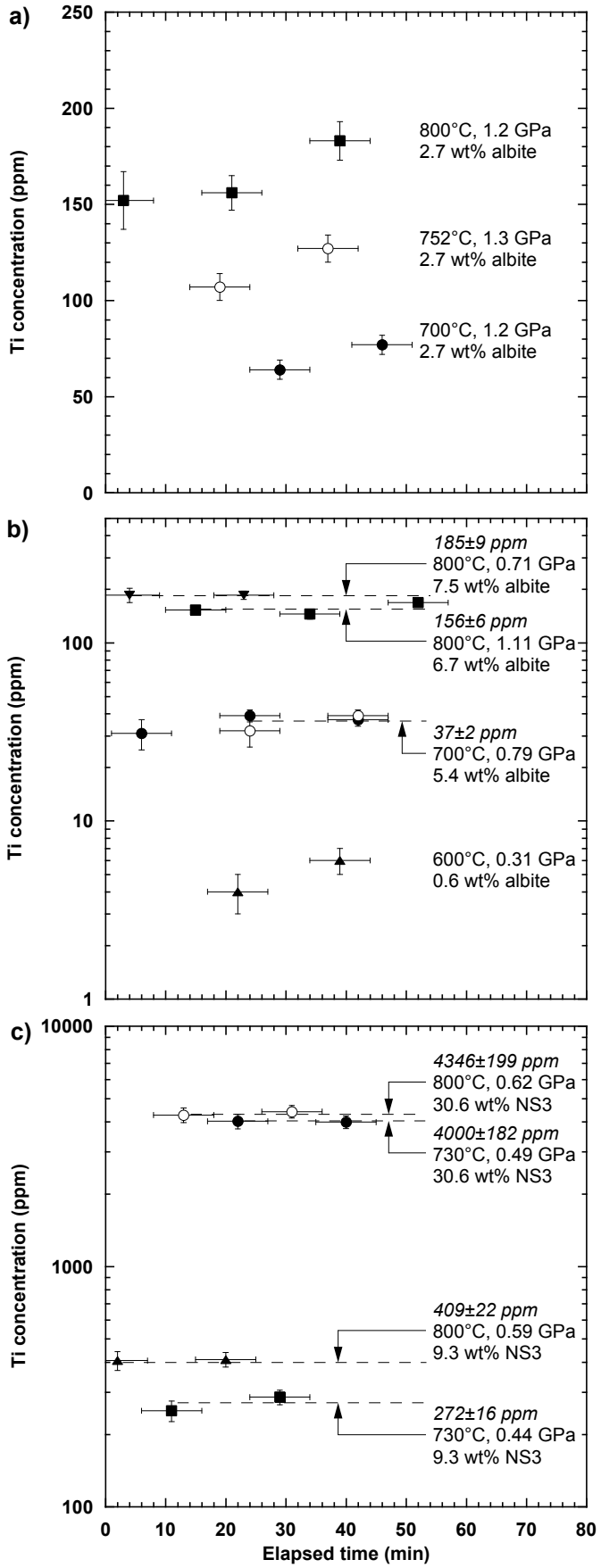

Manning et al., Fig. 3

Figure
Click here to download Figure: fig 4 2.pdf

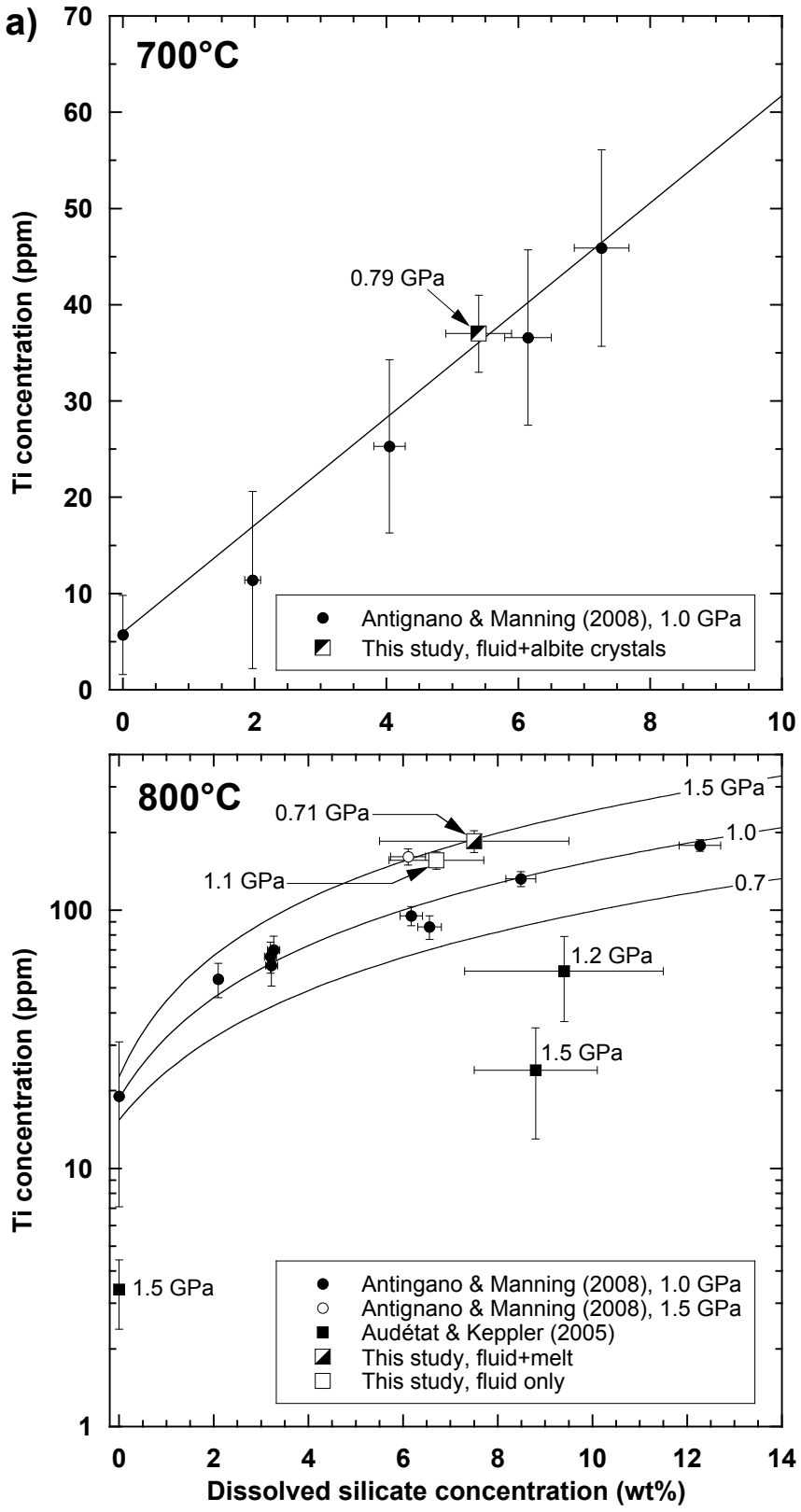

Manning et al., Fig. 4

Figure
Click here to download Figure: fig 5 3.pdf

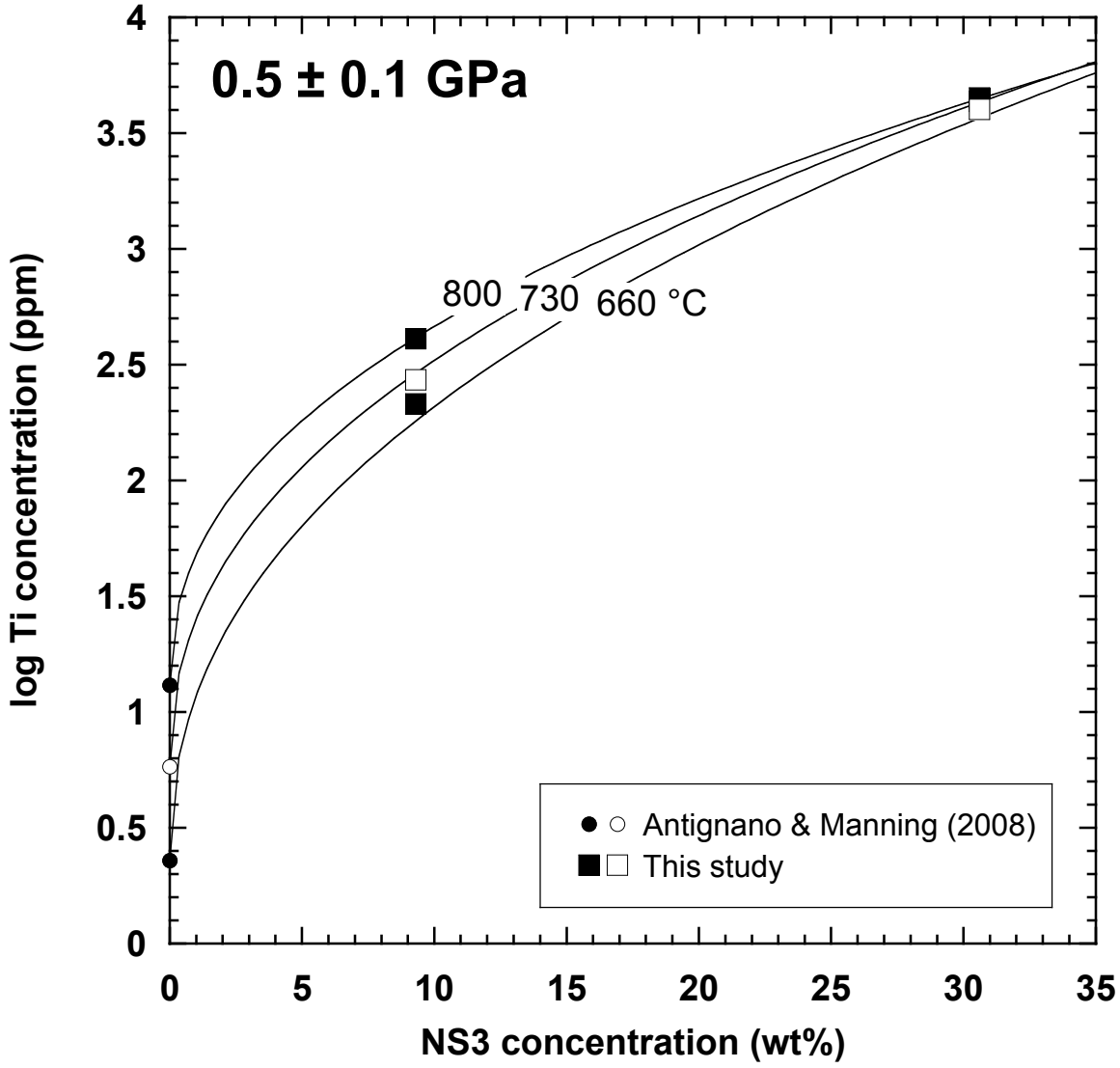

Manning et al., Fig. 5